The source of gypsum in Mammoth Cave, Kentucky

J. Garrecht Metzger, David A. Fike, G. Robert Osburn, Claire J. Guo, and Aaron N. Aadison
Earth and Planetary Sciences, Washington University in St. Louis, Campus Box 1169, 1 Brookings Drive, St. Louis, Missouri 63130, USA

ABSTRACT

Mammoth Cave (Kentucky, USA) is the world's longest human-navigable cave system. Gypsum ($CaSO_4•2H_2O$) crystals line many dry passages of the limestone cave and the source of sulfur for the gypsum remains uncertain. Previous workers have suggested sulfate from pyrite oxidation, Mississippian-aged sulfate evaporites, and Pleistocene soil sulfate as possible sulfur sources. We use sulfur isotopes ($\delta^{34}S$) to constrain the gypsum sulfur source by comparing the $\delta^{34}S$ values of different possible sources to that of gypsum throughout the cave. $\delta^{34}S_{gypsum}$ values (n = 106) from 12 different locations within the Mammoth Cave system are along a continuum of $\delta^{34}S$ values from –12.0‰ to +12.8‰, with little variability along the crystal growth axis or between samples within the same cave chamber. Neither sulfur from coeval sedimentary evaporites (i.e., gypsum, anhydrite) nor from formations overlying the cave is required to explain the $\delta^{34}S_{gypsum}$ data. Rather, the range of pyrite $\delta^{34}S$ in strata immediately surrounding the cave is sufficient to generate the spectrum of observed $\delta^{34}S_{gypsum}$. Modern water $\delta^{34}S_{SO_4}$ values are similar to the host formation $\delta^{34}S_{pyrite}$, suggesting that oxidized pyrite from the host formation continues to be a major sulfur source to this day. Together, these observations strongly suggest a significant local source of sulfur for Mammoth Cave gypsum, the majority (66%–100%) of which is derived from the oxidation of pyrite in strata adjacent to the cave.

INTRODUCTION

Mammoth Cave, located in Kentucky, USA (Fig. 1), is the longest human-navigable cave system in the world, and is more than 640 km in length (Mammoth Cave National Park Service, 2014). Aside from being an important karst terrain, Mammoth Cave is also a U.S. National Park and a United Nations Educational, Scientific and Cultural Organization (UNESCO) World Heritage Site and biosphere reserve. Despite nearly a century of research into the formation of Mammoth Cave and its interior deposits, the origin of the gypsum ($CaSO_4•2H_2O$) that lines cave walls remains uncertain (Weller, 1927; Pohl and Born, 1935; Pohl and White, 1965; Davies and Chao, 1959; George, 1977; Furman et al., 1999; Palmer and Palmer, 2003). The host rock of Mammoth Cave is limestone, which supplies abundant calcium, thereby leaving sulfate as the limiting component for gypsum formation. Several possible sulfate sources were previously suggested, including oxidation of pyrite (FeS_2) from a pyrite-rich layer above the cave (Weller, 1927; Pohl and Born, 1935; Pohl and White, 1965; Furman et al., 1999; Palmer and Palmer, 2003), sulfate mobilized from bedded Mississippian-aged evaporites (gypsum and/or anhydrite; George, 1977), and sulfate leached from Pleistocene soils (Davies and Chao, 1959). A possible alternate source is carbonate-associated sulfate (CAS), where sulfate is substituted for the carbonate ion in the carbonate crystal lattice at ~100–1000 ppm levels (Burdett et al., 1989).

Sulfur isotopes can be used to distinguish between potential sulfur sources because of large offsets in $\delta^{34}S$ values ($\delta^{34}S = [(^{34}S/^{32}S)_{sample}/(^{34}S/^{32}S)_{standard} - 1] \times 10^3$ (‰), relative to the V-CDT [Vienna Canyon Diablo troilite] standard) associated with microbial sulfur cycling (predominantly sulfate reduction), resulting in ^{34}S-depleted sulfides (e.g., pyrites, pyr) and correspondingly ^{34}S-enriched sulfates (e.g., CAS, gypsum, anhydrite). In Phanerozoic sedimentary rocks, $\delta^{34}S_{pyr}$ is typically 30‰–40‰ lower than that of coeval sulfate evaporites and CAS (e.g., Canfield, 2001; Wu et al., 2010). Two gypsum (gyp) samples from Mammoth Cave were previously analyzed (Furman et al., 1999). These values ($\delta^{34}S_{gyp}$ of –5.1‰ and –8.0‰) suggest a significant contribution from oxidized sulfides; however, more samples are needed to characterize spatial patterns in $\delta^{34}S_{gyp}$ throughout the cave, identify any changes in $\delta^{34}S_{gyp}$ over time, and determine the $\delta^{34}S$ of the possible sulfate and sulfide source materials.

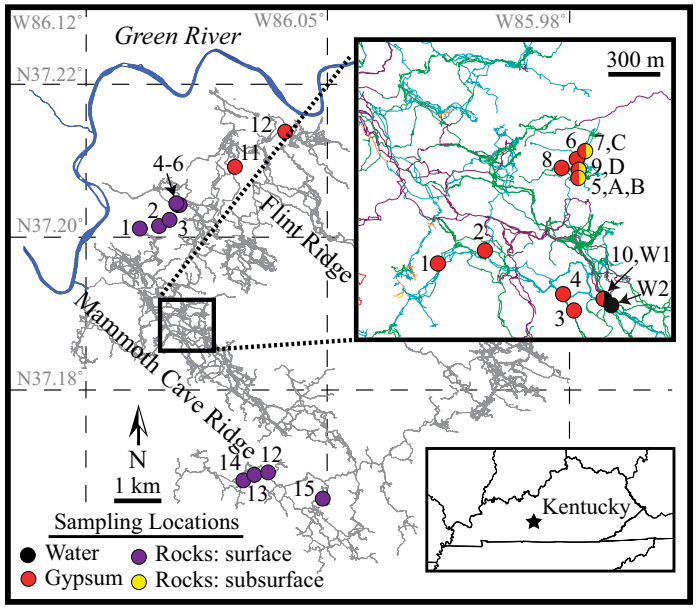

Figure 1. Map of cave passages (gray lines) and sample locations (symbols) within Mammoth Cave National Park (Kentucky, USA). Split symbols represent sampling of multiple materials at scales smaller than resolvable on map. Inset shows subsurface sampling locations from Mammoth Cave Ridge. Colored lines represent relative depth in the cave; from shallowest to deepest, yellow, brown, cyan, green, purple.

Geology of Mammoth Cave

The Mammoth Cave system includes cave passages located within Flint Ridge and Mammoth Cave Ridge (Fig. 1). These ridges are capped by insoluble siliciclastic rocks; limestones line the valleys. Dating of cave sediments using cosmogenic nuclides suggests that the majority of cave formation occurred between 3.62 Ma and 0.85 Ma (Granger et al., 2001; Anthony and Granger, 2007). All strata dip slightly (0.3°–0.5°) to the northwest within the confines of the park, except over localized areas associated with subsurface collapse, jointing, or faulting (Palmer, 1981).

Mammoth Cave is found mostly in the ~110 m of Mississippian-aged Girkin Limestone, Ste. Genevieve Limestone, and St. Louis Limestone (Fig. 2; Palmer, 1981). Most cave passages follow formation or bed boundaries, and the majority of passages occur in the Ste. Genevieve Limestone. The limestones are overlain by the thin and discontinuous Fraileys Shale Member, which is overlain by the Big Clifty Sandstone Member, a thick, quartz-dominated, cross-bedded sandstone with prominent iron staining in outcrop.The Fraileys Shale Member serves as a water seal and gypsum forms only in passages where the overlying Fraileys is absent (e.g., Hess and White, 1989).

Gypsum crystals are found along bedding planes and joints, and gypsum also forms via direct replacement of limestone (White and White, 2003). Gypsum abundance is greatest in formations with known pyrite-rich beds (Palmer and Palmer, 2003). In certain passages of Mammoth

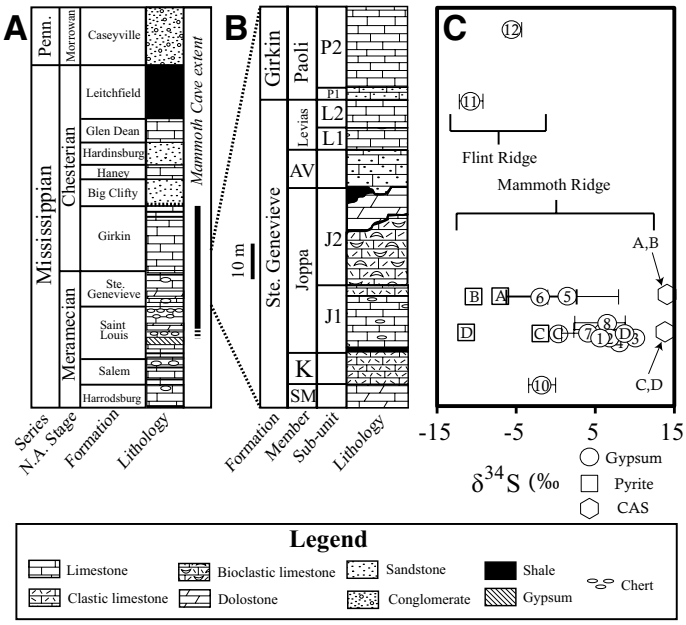

Figure 2. A: Generalized stratigraphic column of Mammoth Cave region (Kentucky, USA) and stratigraphic extent of Mammoth Cave system (modified from Palmer, 1981). B: Generalized stratigraphic column for interval sampled for gypsum and subsurface rocks. AV—Aux Vases, K—Karnak, SM—Spar Mountain. Where blank, subunit designations do not exist. Fraileys Shale Member is a thin, discontinuous unit found at the base of the Big Clifty Sandstone Member. Scale bar refers to B and C only. C: Stratigraphic position of $\delta^{34}S$ data for sample locations corresponding to stratigraphy in B. Numbers are gypsum sample localities and letters are subsurface whole-rock carbonate sample localities. Bars on circles represent total range of $\delta^{34}S$ for gypsum in a given sample location.

Cave, ceiling breakdown is a result of gypsum growth mechanically wedging apart carbonate beds (White and White, 2003).

Many caves with gypsum deposits formed as a result of sulfuric acid-induced dissolution, such as Carlsbad Caverns (New Mexico, USA; Palmer, 2007), Lechuguilla Cave (New Mexico, USA; Jagnow et al., 2000), and the Frasassi Cave system (Italy; Galdenzi et al., 2008). However, Mammoth Cave is an epigenic cave and predominantly formed by carbonate dissolution from carbonic acid– and organic acid–bearing groundwater at low temperature. Sulfuric acid resulting from the oxidation of pyrite is known to play a part in speleogenesis in some caves, but likely played a minor role in Mammoth Cave.

MATERIALS AND METHODS

Gypsum samples (n = 106) were collected from 12 locations within the Mammoth Cave system (Figs. 1 and 2). When possible, sampling included multiple gypsum clusters within the same chamber, separated by a few meters. Due to park regulations, gypsum crystals and subsurface rock samples were limited to those that had fallen to the cave floor. Sample locations were carefully selected for passages where it was clear that materials had not been transported laterally. Gypsum crystal morphologies were varied, including needles, crusts, and blades (Fig. DR1 in the GSA Data Repository[1]). Rock samples representing the relevant strata were collected from the surface (n = 16) and subsurface (n = 4) for $\delta^{34}S$ analyses. Surface samples were collected as close to the studied cave passages as outcrop availability permitted (Fig. 1). Water samples were collected from a small pool 8 m below a low-flow water input and another from a low-flow sulfide seep (Fig. 1).

RESULTS

Stratigraphic trends are found in the $\delta^{34}S_{gyp}$ record (Fig. 2). The lowest $\delta^{34}S_{gyp}$ values are found in the uppermost Ste. Genevieve and lower Girkin Limestones, whereas the highest $\delta^{34}S_{gyp}$ values are in the lower J1 member of the Ste. Genevieve Limestone (Fig. 2). Spatially, $\delta^{34}S_{gyp}$ is lowest in regions underneath Flint Ridge. Variability in $\delta^{34}S_{gyp}$ for a given sampling location was small (0.5‰–3.6‰).

The $\delta^{34}S$ range was different for each sulfur component (Fig. 3A). $\delta^{34}S_{gyp}$ ranged from −12.0‰ to +12.8‰ (average, avg. = 3.3‰, n = 106), $\delta^{34}S_{pyr}$ ranged from −40.7‰ to +17.4‰ (avg. = −2.3‰, n = 15), and $\delta^{34}S_{CAS}$ ranged from 12.6‰ to 17.3‰ (avg. = 15.2‰, n = 12). $\delta^{34}S_{CAS}$ values are similar to coeval Mississippian-aged sulfate evaporites (14‰–19‰; Claypool et al., 1980; Krothe and Libra, 1983) and both have almost no overlap with the observed $\delta^{34}S_{gyp}$ values. High $\delta^{34}S_{pyr}$ values (−2.2‰ to +17.8‰, avg. = 8.7‰, n = 6) were observed for the formations that overlie the cave system (Caseyville Formation, Hardinsburg Sandstone, Big Clifty Sandstone Member, and Fraileys Shale Member; Fig. 3A). Two gypsum-encrusted rock samples from the subsurface Ste. Genevieve Limestone contained sufficient pyrite and CAS for isotopic analyses (Fig. DR3). These two rocks show similar $\delta^{34}S_{CAS}$, but different $\delta^{34}S_{pyr}$ and $\delta^{34}S_{gyp}$.

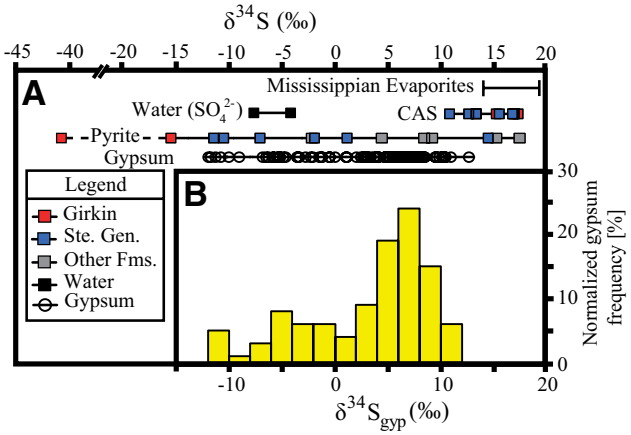

Figure 3. A: $\delta^{34}S$ range of different materials from this study and coeval Mississippian evaporites (Krothe and Libra, 1983). X axis as in B. Dashed line for pyrite samples indicates no samples between lowest (–40.7‰) and next lowest sample (–15.4‰); note break in scale. Other formations (Fms) include Caseyville Formation, Hardinsburg Sandstone, Big Clifty Sandstone Member, and Fraileys Shale Member. Data are listed in Table DR2 (see footnote 1). CAS—carbonate-associated sulfate; Gen.—Genevieve. B: Histogram shows $\delta^{34}S_{gyp}$ frequency grouped into 2.0‰ wide bins.

In the cave water samples, sulfide concentrations were too low to yield enough sulfide for isotopic analysis. However, aqueous $\delta^{34}S_{SO_4}$ was −7.7‰ at the pool and averaged −4.3‰ at the sulfur seep (Fig. 3). These aqueous sulfate $\delta^{34}S_{SO_4}$ values are similar to the average $\delta^{34}S_{pyr}$ (−8.9‰) from the major cave-forming units, the Girkin and Ste. Genevieve Limestones, and slightly lower than average $\delta^{34}S_{pyr}$ (−2.5‰) in the Ste. Genevieve Limestone, the host formation of the water samples.

DISCUSSION

There is little isotopic fractionation (~1.5‰) during abiotic gypsum formation (Thode et al., 1961; Raab and Spiro, 1991) or pyrite oxidation (Field, 1966), so that $\delta^{34}S_{gyp} \approx \delta^{34}S_{source}$. A comparison of $\delta^{34}S$ data from gypsum and the various sulfur sources (Fig. 3A) shows that the range in

[1]GSA Data Repository item 2015067, Figures DR1–DR3 (supplemental figures), and Tables DR1–DR3 (stratigraphic and geochemical information), is available online at www.geosociety.org/pubs/ft2015.htm, or on request from editing@geosociety.org or Documents Secretary, GSA, P.O. Box 9140, Boulder, CO 80301, USA.

$\delta^{34}S_{gyp}$ is within that of $\delta^{34}S_{pyr}$ and has very little overlap with $\delta^{34}S_{CAS}$ or $\delta^{34}S_{evaporite}$. This suggests that, at the scale of the cave system as a whole, the entire range in $\delta^{34}S_{gyp}$ can be explained solely by pyrite oxidation. Variable $\delta^{34}S_{gyp}$ can also result from the mixing of pyrite with other sulfur sources, but the abundance of $\delta^{34}S_{gyp}$ values lower than $\delta^{34}S_{CAS}$ and $\delta^{34}S_{evaporite}$ requires that pyrite be at least a partial source in nearly all gypsum.

We use a mixing model (Fig. 4) to constrain the fraction of gypsum sulfur that is derived from pyrite (f_{pyr}) and sulfate sources (i.e., CAS + evaporites). In this model, $\delta^{34}S_{CAS}$ represents all sulfate mineral sources because the ranges in both $\delta^{34}S_{CAS}$ and $\delta^{34}S_{evaporite}$ are small, and they overlap (Fig. 3A). The relationship between $\delta^{34}S_{pyr}$ and the abundance ratio of pyrite sulfur to total sulfur in gypsum (f_{pyr}) is

$$\delta^{34}S_{pyr} = \frac{\delta^{34}S_{gyp} - \delta^{34}S_{CAS}\left(1 - f_{pyr}\right)}{f_{pyr}}, \quad (1)$$

where $\delta^{34}S_{CAS}$ is the average measured value (14.8‰), $\delta^{34}S_{gyp}$ is a given value within the range of observed values, and f_{pyr} varies from 0 to 1. If we consider average $\delta^{34}S_{pyr}$ from the cave-hosting formations (–8.9‰) and average $\delta^{34}S_{gyp}$ (3.3‰), then f_{pyr} = 0.66 so that 66% of sulfate in the average gypsum crystal (3.3‰) is derived from pyrite. This average f_{pyr} is likely a conservative estimation of the true f_{pyr} because $\delta^{34}S_{pyr}$ brackets the entire range of $\delta^{34}S_{gyp}$, while $\delta^{34}S$ of the sulfate sources have little to no overlap.

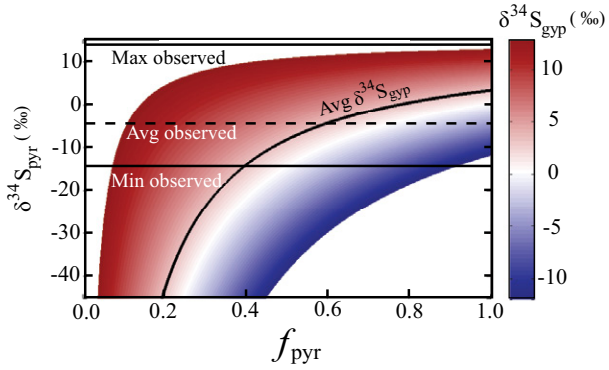

Figure 4. Mixing model showing required fraction of pyrite-sourced sulfur at a given $\delta^{34}S_{pyr}$ (pyr—pyrite; gyp—gypsum) to obtain a particular $\delta^{34}S_{gyp}$ (colored), assuming remaining component is carbonate-associated sulfate (CAS) with $\delta^{34}S_{CAS}$ = 14.8‰. Horizontal lines are observed $\delta^{34}S_{pyr}$ values omitting one outlier at –40.7‰. Intersection of observed average (Avg; Max—maximum; Min—minimum) $\delta^{34}S_{pyr}$ and average $\delta^{34}S_{gyp}$ is at fraction of gypsum sulfur that is derived from pyrite (f_{pyr}) = 0.66 and suggests that the majority of sulfur in the average gypsum crystal is from pyrite oxidation.

Spatial Trends in $\delta^{34}S_{gyp}$, $\delta^{34}S_{pyr}$, and $\delta^{34}S_{CAS}$

$\delta^{34}S_{gyp}$ varies across the cave. There is a stratigraphic pattern in $\delta^{34}S_{gyp}$, increasing with depth over 1–10 m (with the exception of location 10; Fig. 2). Variable $\delta^{34}S_{gyp}$ could be explained by parallel trends in $\delta^{34}S_{pyr}$ (when f_{pyr} is constant), which can explain the low $\delta^{34}S_{pyr}$ and $\delta^{34}S_{gyp}$ values in the Girkin Limestone (Fig. 2C; Table DR2). Coherent stratigraphic variability in $\delta^{34}S_{pyr}$ is well documented in the rock record (e.g., Jones and Fike, 2013). Spatially, $\delta^{34}S_{gyp}$ is lowest in regions underneath Flint Ridge. This is associated with the Ste. Genevieve Limestone–Girkin Limestone boundary. $\delta^{34}S_{CAS}$ is a few permil lower in the subsurface samples. This may result from the increased oxidation of pyrite in the karsted subsurface where subsequent recrystallization of calcite incorporates minor amounts of ^{34}S-depleted sulfate.

Two subsurface rocks from the cave contained all three sulfur phases, yielding information on $\delta^{34}S_{gyp}$, $\delta^{34}S_{pyr}$, $\delta^{34}S_{CAS}$, and f_{pyr} variability over the scale of centimeters (Fig. DR3). The samples yielded different $\delta^{34}S_{gyp}$, $\delta^{34}S_{pyr}$, and f_{pyr}, but very similar $\delta^{34}S_{CAS}$ values. The lack of consistent isotopic relationships may result from differences in $\delta^{34}S_{pyr}$ or f_{pyr} at the centimeter scale. The apparent variability in f_{pyr} could result from spatial variability in $\delta^{34}S_{pyr}$, which is known to vary over micrometers to meters (e.g., Aller et al., 2010; Fischer et al., 2014), a signal superimposed over a coherent meter-scale stratigraphic signal. The data are consistent with variable $\delta^{34}S_{pyr}$ as the main source of $\delta^{34}S_{gyp}$ variability, but cannot exclude f_{pyr} as an additional control. $\delta^{34}S$ data, placed in the context of a gypsum formation model, can further constrain the sulfur source.

Short- Versus Long-Distance Sulfur Transport

Palmer and Palmer (2003) observed gypsum abundance being greatest in passages near pyrite-rich beds and gypsum growth nucleated on iron oxides, interpreted as pyrite oxidation products (Palmer, 2007); the latter is clear evidence that pyrite oxidation can be a local source of gypsum sulfur. This does not, however, establish how much pyrite sulfur contributes to gypsum over the cave system as a whole or the transport history of the sulfur. Palmer and Palmer (2003) proposed a capillary action model of gypsum precipitation where evaporation at the cave wall pores drives gypsum growth. Oxic groundwater passes through the cave wall and oxidizes pyrite sulfur into sulfate. Oxidation of pyrite at typical concentrations (0.01–0.001 wt%) only needs to occur within the first 5–18 m of wall rock to produce gypsum in quantities similar to those observed in Mammoth Cave.

Capillary gypsum formation in pyrite-bearing limestone will not produce gypsum with a $\delta^{34}S$ value dominated by CAS because large percentages of the limestone must be dissolved to release sufficient CAS. Oxic groundwater could travel through the cave wall or oxygen could diffuse into the cave wall and oxidize pyrite, while CAS release would require acidic groundwater that breaks down the cave wall. The lack of Mn oxides near gypsum crystals is evidence that the groundwater near the cave wall is oxic rather than anoxic.

The capillary action model of gypsum formation suggests that sulfur transport distance need only be ~10 m within the cave wall to form gypsum in quantities similar to that observed in Mammoth Cave. This is consistent with $\delta^{34}S_{pyr}$ data, which show that no sulfur (CAS, evaporites, or pyrite) from formations overlying the cave is required to explain the $\delta^{34}S_{gyp}$ values. Because pore waters pass through the cave wall immediately adjacent to the gypsum, they will inherit at least some characteristics of the local geochemistry and, by extension, pore water sulfate would undergo isotopic homogenization as it travels toward the cave wall. This would result in a $\delta^{34}S_{gyp}$ range smaller than the $\delta^{34}S_{pyr}$ range, which is consistent with our observations (Fig. 3). While the range in $\delta^{34}S_{gyp}$ is smaller than the range in $\delta^{34}S_{pyr}$, the $\delta^{34}S_{gyp}$ range remains large due to minimal transport and mixing. We suggest that the lack of consistent $\delta^{34}S_{gyp}$, $\delta^{34}S_{pyr}$, and f_{pyr} values at the centimeter scale (Fig. DR3) results from the averaging of pyrite sulfur during transport, which occurs at the meter scale.

Gypsum Formation Through Time

Cave formation at Mammoth likely occurred during the past 3.5 m.y. (Granger et al., 2001; Anthony and Granger, 2007). Gypsum could precipitate in passages once flowing water had receded, but it is unknown precisely when or how quickly gypsum precipitated in the cave. Certain cave locations, such as Giant's Coffin and Snowball Dining Room, where human signatures are etched into the wall gypsum, show minor regrowth (R.S. Toomey, 2014, personal commun.), suggesting that some gypsum could have formed in the past few hundred years. The $\delta^{34}S_{gyp}$ values observed along the growth axis for single gypsum crystals (Fig. DR2) are consistent with a constant sulfur source through time. It is not possible to sample water that is actively precipitating gypsum in the cave because gypsum growth is associated with trace quantities of water, so water found in close proximity to gypsum-bearing passages is the closest approxima-

tion. The $\delta^{34}S_{SO_4}$ from water samples (–6.0‰) is very similar to the average $\delta^{34}S_{pyr}$ from the host formation of the water samples. These data are consistent with a local (at the formation or member level) source of dissolved sulfur and gypsum sulfur, suggesting that pyrite sulfur continues to be a significant sulfur source in Mammoth Cave today.

SUMMARY

The $\delta^{34}S$ data and geologic context strongly suggest that pyrite is the dominant, and in some cases exclusive, sulfate source for modern cave waters and gypsum. Contributions from carbonate-associated sulfate (CAS) and evaporites to Mammoth Cave gypsum must be minimal. Invariant $\delta^{34}S$ along the growth axis of single gypsum crystals suggests that this has been the case throughout the growth history of the gypsum. A mixing model suggests that for the average gypsum crystal, >66% of sulfur is derived from pyrite. The overlap between $\delta^{34}S$ of pyrite and gypsum at a given stratigraphic level, the large range of isotopic variability in these signals, and the mode of gypsum formation suggests that proximal pyrite (within 1–20 m) is the dominant gypsum sulfur source, in agreement with Palmer and Palmer (2003). This work provides insight into gypsum speleogenesis and hydrology in Mammoth Cave and may be important for understanding sulfate speleogenesis in other epigenic limestone caves and karst regions (e.g., Berome Moore Cave in Missouri, Fitton Cave in Arkansas, and caves in the Cumberland Plateau escarpment in Tennessee).

ACKNOWLEDGMENTS

We thank the U.S. National Park Service for permission to undertake this study (NPS permit MACA-2010-SCI-0014). We also thank R. Toomey, R. Olson, and B. Hatcher for their assistance with sampling, and A. Palmer and P. Palmer for help in identification of stratigraphic members. Metzger thanks B. Gilhooly for advice on water collection, and M. Brasher and J. Gao for assistance with S extractions. This study was funded by a Packard Fellowship to Fike.

REFERENCES CITED

Aller, R., Madrid, V., Chistoserdov, A., Aller, J.Y., and Heilbrun, C., 2010, Unsteady diagenetic processes and sulfur biogeochemistry in tropical deltaic muds: Implications for oceanic isotope cycles and the sedimentary record: Geochimica et Cosmochimica Acta, v. 74, p. 4671–4692, doi:10.1016/j.gca.2010.05.008.

Anthony, D.M., and Granger, D.E., 2007, A new chronology for the age of the Appalachian erosional surfaces determined by cosmogenic nuclides in cave sediments: Earth Surface Processes and Landforms, v. 32, p. 874–887, doi:10.1002/esp.1446.

Burdett, J.W., Arthur, M.A., and Richardson, M., 1989, A Neogene seawater sulfur isotope age cure from calcareous pelagic microfossils: Earth and Planetary Science Letters, v. 94, p. 189–198, doi:10.1016/0012-821X(89)90138-6.

Canfield, D.E., 2001, Biogeochemistry of sulfur isotopes, *in* Valley, J.W., and Cole, D.R., eds., Stable isotope geochemistry: Mineralogical Society of America Reviews in Mineralogy and Geochemistry Volume 43, p. 607–636, doi:10.2138/gsrmg.43.1.607.

Claypool, G.E., Holser, W.T., Kaplan, I.R., Sakai, H., and Zak, I., 1980, The age curves of sulfur and oxygen isotopes in marine sulfate and their mutual interpretation: Chemical Geology, v. 28, p. 199–260, doi:10.1016/0009-2541(80)90047-9.

Davies, W.E., and Chao, E.C.T., 1959, Report on sediments in Mammoth Cave, Kentucky: U.S. Geological Survey Administrative Report, 117 p.

Field, C.W., 1966, Sulfur isotopic method for discriminating between sulfates of hypogene and supergene origin: Economic Geology and the Bulletin of the Society of Economic Geologists, v. 61, p. 1428–1435, doi:10.2113/gseconge o.61.8.1428.

Fischer, W.W., Fike, D.A., Johnson, J.E., Raub, T.D., Guan, Y., Kirschvink, J.L., and Eiler, J.M., 2014, SQUID-SIMS is a useful approach to uncover primary signals in the Archean sulfur cycle: National Academy of Sciences Proceedings, v. 111, p. 5468–5473, doi:10.1073/pnas.1322577111.

Furman, F.C., Gregg, J.M., Palmer, A.N., and Shelton, K.L., 1999, Sulfur isotopes of gypsum speleothems in Central Kentucky Karst System: Indications of pyrite and anhydrite sulfur sources, and sulfuric acid karstification: MSM Spelunker, v. 42, p. 20–24.

Galdenzi, S., Cocchioni, M., Morichetti, L., Amici, V., and Scuri, S., 2008, Sulfidic ground-water chemistry in the Frasassi Caves, Italy: Journal of Caves and Karst Studies, v. 70, p. 94–107.

George, A.I., 1977, Evaluation of sulfate water quality in north-central Kentucky karst, *in* Dilamarter, R.R., and Csallany, S.C., eds., Hydrologic problems in karst regions: Bowling Green, Western Kentucky University, p. 340–356.

Granger, D.E., Fabel, D., and Palmer, A.N., 2001, Pliocene–Pleistocene incision of the Green River, Kentucky, determined from radioactive decay of cosmogenic ^{26}Al and ^{10}Be in Mammoth Cave sediments: Geological Society of America Bulletin, v. 113, p. 825–836, doi:10.1130/0016-7606(2001)113<0825:PPIOTG>2.0.CO;2.

Hess, J.W., and White, W.B., 1989, Chemical hydrology, *in* White, W.B., and White, E.L., ed., Karst hydrology: Concepts from the Mammoth Cave area: New York, Van Nostrand Reinhold, p. 145–174.

Jagnow, D.H., Hill, C.A., Davis, D.G., DuChene, H.R., Cunningham, K.I., Northup, D.E., and Queen, J.M., 2000, History of the sulfuric acid theory of speleogenesis in the Guadalupe Mountains, New Mexico: Journal of Caves and Karst Studies, v. 62, p. 54–59.

Jones, D.S., and Fike, D.A., 2013, Dynamic sulfur and carbon cycling through the end-Ordovician extinction revealed by paired sulfate-pyrite $\delta^{34}S$: Earth and Planetary Science Letters, v. 363, p. 144–155, doi:10.1016/j.epsl.2012.12.015.

Krothe, N.C., and Libra, R.D., 1983, Sulfur isotopes and hydrochemical variations in spring waters of southern Indiana, U.S.A.: Journal of Hydrology, v. 61, p. 267–283, doi:10.1016/0022-1694(83)90253-6.

Mammoth Cave National Park Service, 2014, Park news: http://www.nps.gov/maca/parknews/mammoth-cave-400-miles.htm (March 2014).

Palmer, A.N., 1981, A geological guide to Mammoth Cave National Park: Teaneck, New Jersey, Zephyrus Press, 210 p.

Palmer, A.N., 2007, Cave geology: Dayton, Ohio, Cave Books, 454 p.

Palmer, A.N., and Palmer, M.V., 2003, Geochemistry of capillary seepage in Mammoth Cave: 4th Mammoth Cave Science Conference, Volume 1: Mammoth Cave, Kentucky, International Union of Speleology and International Association of Hydrogeologists, p. 1–8.

Pohl, E.R., and Born, K.M., 1935, Development of gypsum in limestone caves [abs.], *in* Proceedings, Geological Society of America 48th Annual Meeting, New York: New York, Geological Society of America, p. 96.

Pohl, E.R., and White, W.B., 1965, Sulfate minerals: Their origin in the central Kentucky karst: American Mineralogist, v. 50, p. 1461–1465.

Raab, M., and Spiro, B., 1991, Sulfur isotopic variations during seawater evaporation with fractional crystallization: Chemical Geology, v. 86, p. 323–333, doi:10.1016/0168-9622(91)90014-N.

Thode, H.G., Monster, J., and Dunford, H.B., 1961, Sulfur isotope geochemistry: Geochimica et Cosmochimica Acta, v. 25, p. 159–174, doi:10.1016/0016-7037(61)90074-6.

Weller, J.M., 1927, The geology of Edmonson County, Kentucky: Kentucky Geological Survey Report 28, 246 p.

White, W.B., and White, E.L., 2003, Gypsum wedging and cavern breakdown: Studies in the Mammoth Cave System, Kentucky: Journal of Caves and Karst Studies, v. 65, p. 43–52.

Wu, N., Farquhar, J., Strauss, H., Kim, S., and Canfield, D.E., 2010, Evaluating the S-isotope fractionation associated with Phanerozoic pyrite burial: Geochimica et Cosmochimica Acta, v. 74, p. 2053–2071, doi:10.1016/j.gca.2009.12.012.

Manuscript received 28 July 2014
Revised manuscript received 8 December 2014
Manuscript accepted 9 December 2014

Printed in USA